Article

Modal Aggregation Technique to Check the Accuracy of the Model Reduction of Array Cable Systems in Offshore Wind Farms

Mohammad Kazem Bakhshizadeh [1,*], Benjamin Vilmann [1,2] and Łukasz Kocewiak [1]

[1] Ørsted Wind Power A/S, 7000 Fredericia, Denmark
[2] Department of Wind and Energy Systems, Technical University of Denmark, 2800 Kongens Lyngby, Denmark
* Correspondence: modow@orsted.com

Abstract: The need for a verification method for aggregation techniques for passive electrical systems is necessary as power systems increase in complexity. Model reduction is crucial to increase the number of simulations necessary to ensure a stable and reliable design of power systems. This paper presents a novel modal domain-based technique to identify the best aggregation technique for a given system and to indicate the validity of the aggregation. This is done by benchmarking different aggregation techniques and using the dominant contribution factor ratio as a validity parameter. The different aggregation techniques are compared via time-domain simulations against the full detailed model. It is found that (1) the power loss aggregation technique is the most precise when it weighs the equivalent impedances of the parallel feeders, (2) unequal current generation does not impact the aggregation accuracy, (3) individual string aggregation provides the best results for dynamic simulations, and (4) the validity of aggregation decreases as frequency or cable length increases.

Keywords: modal; eigenvalue-based; model reduction; aggregation; offshore wind farm; collector system

1. Introduction

Model reduction of wind farms has been a subject of interest since the early 1990's [1]. Recent studies shows an ongoing demand for sound aggregated wind farm models [2]. The need for a verification method for aggregation techniques for passive electrical systems for offshore wind farms (OWF) is evident. There is also a need for an indication of the validity of the aggregation. This paper presents a novel modal aggregation technique that serves both purposes. The proposed modal aggregation technique is, however, only looking into the collector system of offshore wind farm power systems. The aggregation of the collector system might also be relevant for active distribution networks (ADN), as these also consider wind farms equivalents [3].

Much research has been conducted looking into full-aggregation of doubly-fed induction generator-based (DFIG) OWFs. The DFIG has been a popular wind turbine (WT) as it was the most frequently installed WT type from 2001 to 2004 world wide (Data is available from 1995 to 2004.) [4]. A dynamic model equivalent has been developed by the swing equation in [5,6]. A similar dynamic model is developed in [7] but by utilizing the flux linkage of the machine. The wind profile is furthermore included in [8].

A German trend analysis of installed WT per type each year shows that the type-4 WT gained interest and accounts for at least 50 % of the installed WTs since 2010 (Data is available from 1998 to 2018.) [9]. In [10], a wind profile-based full-aggregated dynamic model equivalent is developed for the type-4 WT. It is however reported that full-aggregation methods neglect the internal oscillatory behavior and dynamics [11]. Furthermore, it is claimed that the nonlinear power production and inertial response are neglected due to wake effects [12], and the non-uniform wind speed distribution across the OWF [13]. However, the semi-aggregation accommodates some non-uniformity in the model reduction

either by the WT model aggregation [14] or by representing the OWF by a multi-machine aggregated model [15–17].

The multi-machine representation supports modal analysis, coherency analysis, and various clustering methods. An argument against these aggregation techniques is that they might ignore the electrical distance, i.e., a coherency analysis could find a common mode for two WTs in different strings [11].

Aggregation of wind farms tends to neglect the system harmonics. Ref. [18] investigates several methods to aggregate harmonic current emissions from WTs for prediction of power system harmonics by coupling the DC-link voltage and the PLL. This aggregation requires insight of the WT model itself, however.

Designing OWFs often involves collaboration with WT suppliers, who deliver black-boxed WT models. Thus, there is a distinction between a certain parameter-based model aggregation of white-boxed models and identified parameter-based model aggregation of black-boxed models. Parameters can be identified by optimization algorithms like particle swarm optimization [19]. Another approach would be to perform vector fitting to the entire wind farm dynamics, as proposed in [18]. An option is to develop a grey-box model that allows a dynamic equivalent model order reduction by parameter estimation in ADNs [3,20].

As a draw-back, grey-boxing loses some of the traceability of the system parameters and dynamics. This is the motivation for investigating the aggregation techniques of the passive system alone, i.e., the collector system (CS) of the OWF, as it is independent of the wind turbine type and the level of model transparency.

In [21–23], a voltage drop-based analysis of the equivalent string impedance in the collector system is considered. In [24–28], a similar approach is noted, but the individual impedance is weighted with respect to a consideration of power losses. Ref. [29] proposes the short-circuit impedance given by the short-circuit level (SCL) of the OWF as the equivalent impedance of the entire system. Because the latter aggregation technique is based on doubly-fed induction machines (DFIGs), it will not be benchmarked as the aggregation technique bases on a specific type of WT.

The paper is organized in the following manner: Section 2 presents the theory of the proposed modal aggregation technique. Section 4 defines the benchmarked aggregation techniques and the immediate differences. Section 3 outlines the case studies in terms of tests, dimensions of the OWF, and the model setup. Diverse wind farm layouts are discussed in [30–32] but none of the aggregation techniques covers how branches in the individual strings are handled. The paper will thus benchmark the performance with respect to the existence of branches in the strings. Section 5 shows and elaborates the results of the time-domain simulations. Section 6 discusses the validity of aggregation for studies for higher frequencies, for larger impedance, and asymmetric strings. Section 7 concludes on the most accurate aggregation technique, the potential of the dominant contribution factor ratio (DCFR) as a validity parameter of the aggregation, and suggests a validity threshold to the DCFR.

2. Modal Aggregation Technique

Offshore wind farms are an assembly of WTs connected in radial feeders to the offshore substation, which constitutes the collector system. As these array cable systems are in the 33–66 kV range and extend from 2–30 km, many dynamics take place in the collector system [33]. It is desired to preserve the special dynamic response of the system after aggregation, motivated by speeding up the computation of grid interaction studies. In Figure 1a, a high-level OWF model shows the conceptual layout of the WTs in feeders. In Figure 1b, the conceptual equivalent-ready model is illustrated by the assumption of WTs as current sources.
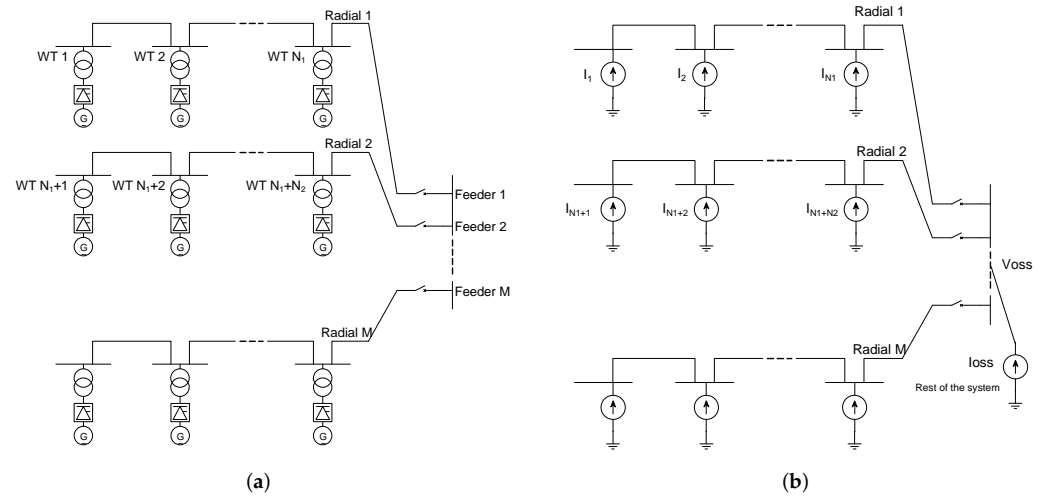
Figure 1. Conceptual OWF model. (**a**) M feeders with N_m WTs in feeder m. (**b**) WTs as current sources.

The aggregation represents the collector system and the power generation from WTs as a single WT representation of the system behind an equivalent RLC component connected to the offshore substation (OSS), as seen in Figure 2:
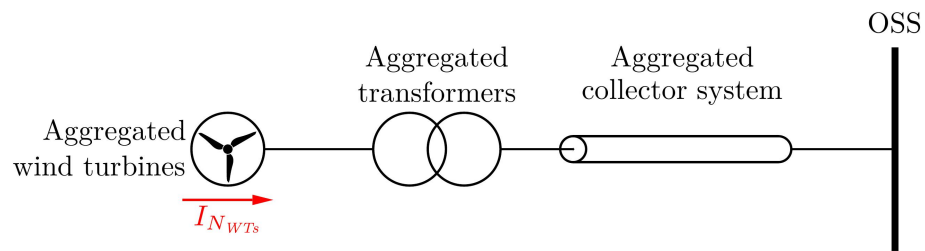

Figure 2. Conceptual aggregated model.

The aggregation can be done by circuit analysis and assumptions on power generation (as it is shown in Section 3). However, the equivalent impedance of the OWF collector system can also be aggregated by eigenvalues and eigenvectors of the system. Recalling relevant theory, it is noted that an eigenvalue λ_i of a matrix $\mathbf{A}$ is associated with the right eigenvector $\mathbf{r}_i$ [34], so that:

$$\mathbf{A}\mathbf{r}_i = \lambda_i \mathbf{r}_i \tag{1}$$

In matrix format, eigenvalues and eigenvectors are given:

$$\mathbf{\Lambda} = \begin{bmatrix} \lambda_1 & \dots & 0 \\ \vdots & \ddots & \vdots \\ 0 & \dots & \lambda_N \end{bmatrix}, \quad \mathbf{R} = \begin{bmatrix} \mathbf{r}_1 & \dots & \mathbf{r}_N \end{bmatrix} \tag{2}$$

Matrix notation allows similar expression as in (1):

$$\mathbf{A}\mathbf{R} = \mathbf{R}\mathbf{\Lambda} \tag{3}$$

where $\mathbf{R}$ is the matrix of the right eigenvectors.

Application

For any CS associated with an OSS, there is $N - 1$ cable sections with respect to N WTs in the cluster(s) (assuming no loops in the array system). The voltages at each node in the investigated system can be given in matrix format:

$$\mathbf{V} = \mathbf{Z}\mathbf{I} \tag{4}$$

where $\mathbf{V} \in \mathbb{C}^{N+1 \times 1}$ is the voltages at each node. $\mathbf{Z} \in \mathbb{C}^{N+1 \times N+1}$ is the impedance matrix of the investigated system. $\mathbf{I} \in \mathbb{C}^{N+1 \times 1}$ is the current injections at each node, all at the fundamental frequency. The matrix can be partitioned for better interpretation as follows:

$$\begin{bmatrix} \mathbf{V}_{WTs} \\ ine\mathbf{V}_{OSS} \end{bmatrix} = \begin{bmatrix} \mathbf{Z}_{CS} & \mathbf{Z}_m \\ ine\mathbf{Z}_m^T & \mathbf{Z}_{OSS} \end{bmatrix} \begin{bmatrix} \mathbf{I}_{WTs} \\ ine\mathbf{I}_{OSS} \end{bmatrix} \tag{5}$$

where $\mathbf{V}_{WTs} \in \mathbb{C}^{N \times 1}$ is the voltage at the WT nodes. $\mathbf{V}_{OSS} \in \mathbb{C}^{1 \times 1}$ is the OSS voltage. $\mathbf{Z}_{CS} \in \mathbb{C}^{N \times N}$ is the partition of the impedance matrix of the system, representing the CS. $\mathbf{Z}_m \in \mathbb{C}^{N \times 1}$ is the mutual impedance of the CS and the OSS. $\mathbf{Z}_{OSS} \in \mathbb{C}^{1 \times 1}$ is the partition of the impedance matrix of the investigated system, which could be associated with the grid. $\mathbf{I}_{WTs} \in \mathbb{C}^{N \times 1}$ is the current injections of the WTs. $\mathbf{I}_{OSS} \in \mathbb{C}^{1 \times 1}$ is the current injection at the OSS. The system matrix $\mathbf{Z}_{CS}$ can be expressed in terms of (3):

$$\mathbf{Z}_{CS} = \mathbf{R}\boldsymbol{\Lambda}_{CS}\mathbf{R}^{-1} \tag{6}$$

The partitioned voltages are thus rewritten:

$$\begin{aligned} \mathbf{V}_{WTs} &= \mathbf{R}\boldsymbol{\Lambda}_{CS}\mathbf{R}^{-1}\mathbf{I}_{WTs} + \mathbf{Z}_m\mathbf{I}_{OSS} \\ \mathbf{V}_{OSS} &= \mathbf{Z}_m^T\mathbf{I}_{WTs} + \mathbf{Z}_{OSS}\mathbf{I}_{OSS} \end{aligned} \tag{7}$$

Modal currents and voltages are defined as:

$$\begin{aligned} \mathbf{V}'_{WTs} &= \mathbf{R}^{-1}\mathbf{V}_{WTs} \\ \mathbf{I}'_{WTs} &= \mathbf{R}^{-1}\mathbf{I}_{WTs} \end{aligned} \tag{8}$$

which leads to (9) by substituting (8) in (7):

$$\begin{aligned} \mathbf{V}'_{WTs} &= \boldsymbol{\Lambda}\mathbf{I}'_{WTs} + \mathbf{R}^{-1}\mathbf{Z}_m\mathbf{I}_{OSS} \\ \mathbf{V}_{OSS} &= \mathbf{Z}_m^T\mathbf{R}\mathbf{I}'_{WTs} + \mathbf{Z}_{OSS}\mathbf{I}_{OSS} \end{aligned} \tag{9}$$

The impact of the modal currents on the OSS voltage from the current injection from the WTs are given by contribution factors (CF) $\mathbf{m}$:

$$\mathbf{m} = \mathbf{Z}_m^T\mathbf{R}\mathbf{I}'_{WTs} \in \mathbb{C}^{N \times 1} \tag{10}$$

It is assumed for the sake of simplicity, that the current of the individual WT is considered to be identical and at nominal generation, i.e., $I_{WT_1} = I_{WT_2} = \ldots = I_{WT_N} = 1\angle 0°$ per-unit (in Section 6.1 it is shown that unequal current in phase and magnitude does not change the conclusion of this method):

$$\mathbf{I}_{WTs} = \begin{bmatrix} 1\angle 0° & 1\angle 0° & \ldots & 1\angle 0° \end{bmatrix}^T \in \mathbb{C}^{N \times 1} \tag{11}$$

It can be shown that in most cases, only one modal current is important, and the other modal currents are much smaller, i.e., $m_0 \gg m_1$. Therefore, (9) can be approximated by only one model current and one modal voltage. Let 0 denote the index of the dominant contribution factor and let $\mathbf{m}$ be sorted in descending order with respect to magnitude:

$$\begin{aligned} \mathbf{V}'_{WTs}[0] &= \boldsymbol{\Lambda}[0,0]\mathbf{I}'_{WTs}[0] + \left(\mathbf{R}^{-1}\mathbf{Z}_m\right)[0]\mathbf{I}_{OSS} \\ \mathbf{V}_{OSS} &= \left(\mathbf{Z}_m^T\mathbf{R}\right)[0]\mathbf{I}'_{WTs}[0] + \mathbf{Z}_{OSS}\mathbf{I}_{OSS} \end{aligned} \tag{12}$$

The investigated system can thus be aggregated into two nodes, namely the OSS and a fictitious node representing the dominant modal voltage and current.

Since the modal currents and voltages are not identical to real currents and voltages, an ideal transformer is introduced to transform the voltage level to the same as before but scale the current up (as expected in an aggregated wind turbine), as seen in Figure 3:
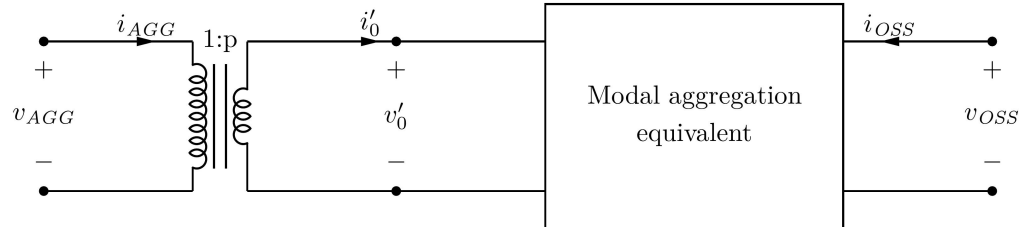

Figure 3. Modal transformer model.

The turn ratio is given by p and defined as:

$$p = \frac{\sum_1^N \mathbf{I}_{WTs,i}}{\mathbf{I}'_{WTs}[0]} \cong \sqrt{N} \tag{13}$$

where $p \in \mathbb{C}^1$. The transformer model enables the construction of the two port aggregated system (AS) by transforming back from modal to real domain:

$$\mathbf{V}_{AS} = \begin{bmatrix} \mathbf{V}_{agg} \\ \mathbf{V}_{OSS} \end{bmatrix} = \begin{bmatrix} \frac{1}{p^2}\mathbf{\Lambda}_{CS}[0,0] & \frac{1}{p}\left(\mathbf{R}^{-1}\mathbf{Z}_m\right)[0] \\ \frac{1}{p}\left(\mathbf{Z}_m^T\mathbf{R}\right)[0] & \mathbf{Z}_{OSS} \end{bmatrix} \begin{bmatrix} \mathbf{I}_{agg} \\ \mathbf{I}_{OSS} \end{bmatrix} = \mathbf{Z}_{AS}\mathbf{I}_{AS} \tag{14}$$

The impedance matrix of the AS is asymmetric and nonreciprocal [35,36], i.e., the current and voltage of one port does not translate into the other port by means of passive electrical components and vice versa. In perspective, phase-shifting transformers are also asymmetric when the phase is different from 0, $\alpha \neq 0$ [37].

3. Case Study

This paper intends to benchmark aggregation techniques against the modal aggregation technique based on different collector system layouts. Therefore, the paper is inspired by the Anholt Wind Farm (400 MW, with 111 WTs of 3.6 MW capacity distributed equally in 12 strings) located in Denmark [38]. The layout of the wind farm is found in [33] and shown in Figure 4. The cable data is taken from [39] and noted in Table 1. Four base study cases are considered for model aggregation to study the behavior. Study case 2 and 4 are also investigated with an unequal number of WTs in each feeder to show the challenges with asymmetry. Layout properties are given in Table 2. The wind farm layout and study cases are shown in Figure 4:

The model of the detailed and aggregated study cases are built in PSCAD 4.6.3. The WT model is a type-4B (includes aerodynamic and mechanical parts [40]) and is publicly available in PSCAD examples [41]. The model used is an averaged model, which disregards switching ripples. The WT model includes fault-ride-through (FRT) capabilities. The grid (OSS node) is modeled by a voltage source behind a grid impedance ($SCR = 20$, $X/R = 10$). All cables are modelled as PI-sections.

Table 1. Array cable data. Source: [39].

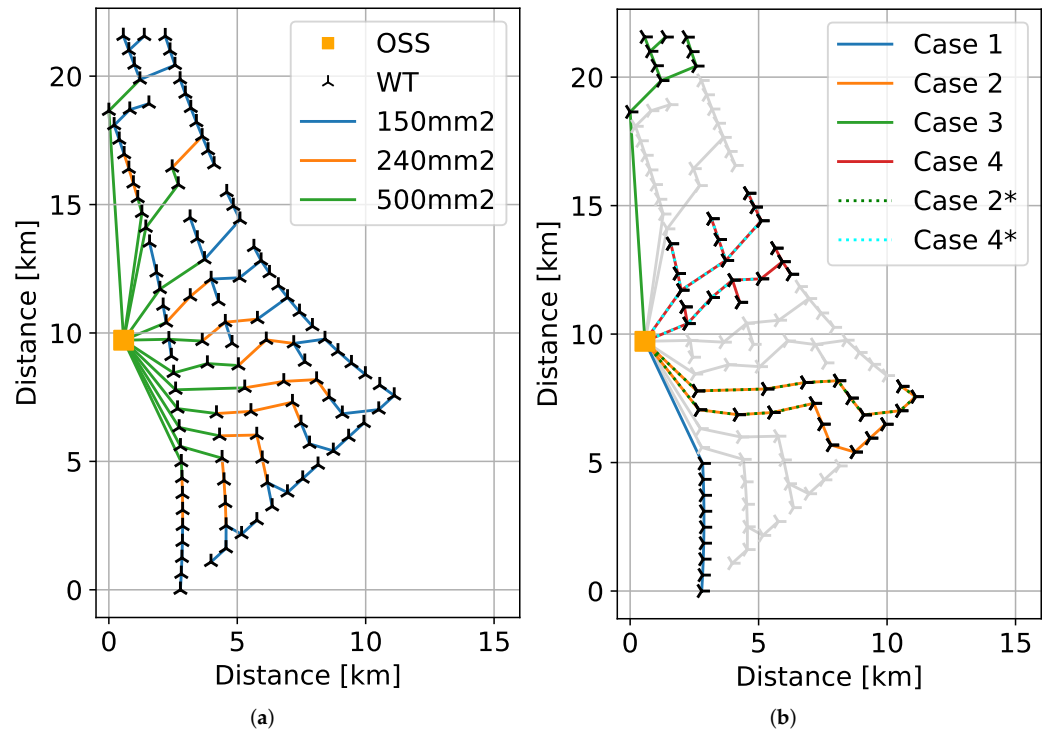| Cable Type	R [mΩ/km]	L [mH/km]	C [μF/km]
150 mm^2	124	0.39	0.19
240 mm^2	75.4	0.36	0.23
500 mm^2	36.6	0.32	0.32

Figure 4. Anholt Wind Farm collector system layout and case designated layouts. (**a**) Collector system layout. (**b**) Case studies.

Table 2. Case study data.

Case	Number of Strings	Branches	Symmetry	N_{WT}	S_{base} [MW]
1	1		✓	9	32.4
2	2		✓	9	32.4
3	1	✓	✓	18	64.8
4	2	✓	✓	18	64.8
2*	2			13	46.8
4*	2	✓		13	46.8

To compare the aggregation accuracy and precision, the dynamic behavior of the system is investigated in time-domain by applying a 3-phased bolted fault to ground at the OSS. The aggregated model implemented in PSCAD is shown in Figure 5:
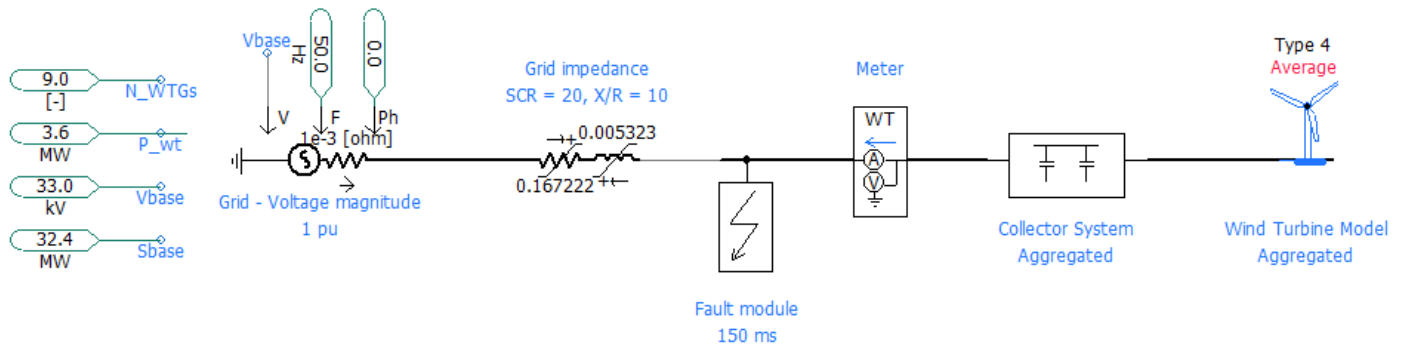

Figure 5. Representation of the aggregated system in time-domain simulation studies in PSCAD.

4. Aggregation Techniques

4.1. Benchmarked Aggregation Techniques

The voltage drop [21–23], the power loss #1 [42], and the power loss #2 [22,24,28] aggregation techniques use weighting of the individual impedance with respect to the amount of current injected that it carries (per unit) (The IDs added for the power loss methods is our notation.). In Figure 1a, an OWF is represented by M feeders, with corresponding N_m WTs of the individual feeder, m. In Figure 1b, it is shown that the WT itself is simplified with a current source connected to the grid bus with the voltage v_g and an associated current source, representing current injections from the grid, i_g.

The aggregation of feeder m is denoted as Z_m and the aggregation of all feeders are denoted as Z_{eq}. The graph model of the system considers a weighting of each cable section as shown in Figure 6 for an offshore substation (OSS) with two strings. In one of the strings, there are branches, and a basic array of WTs in the other. The example shows an asymmetry in number of WTs per string.
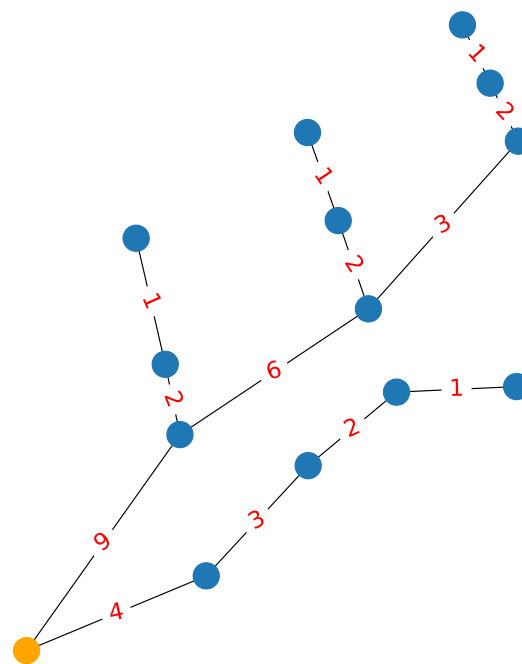

Figure 6. Example of a weighted graph (Case 4 *).

The mentioned aggregation techniques are shown in Table 3. It is seen that the equivalent impedance of each feeder Z_m is based on the weighting of each cable section (exemplified in Figure 6). The weighting term for the voltage drop method is based on the relation $V = IZ$. The power loss method is based on the relation $P = I^2Z$ in contrast.

Table 3. Current based aggregation techniques.

	Voltage Drop (VD)		Power Loss #1 (PL1)		Power Loss #2 (PL2)	
Z_m: Equivalent impedance of the individual feeder, m	$Z_m = \frac{1}{N_m} \sum_n^{N_m} w_n Z_{n,m}$	(15)	$Z_m = \frac{1}{N_m^2} \sum_n^{N_m} w_n^2 Z_{n,m}$	(16)	$Z_m = \frac{1}{N_m^2} \sum_n^{N_m} w_n^2 Z_{n,m}$	(17)
Z_{eq}: Equivalent impedance of the whole wind farm	$Z_{eq} = \frac{1}{\sum_{i=1}^M \frac{1}{Z_m}}$	(18)	$Z_{eq} = \frac{1}{\sum_{i=1}^M \frac{1}{Z_m}}$	(19)	$Z_{eq} = \frac{\sum_m^M N_m^2 Z_m}{\left[\sum_m^M N_m\right]^2}$	(20)
C_{eq}: Equivalent capacitance of the whole wind farm	$C_{eq} = \sum_m^M \sum_n^{N_m} C_{n,m}$	(21)	$C_{eq} = \sum_m^M \sum_n^{N_m} C_{n,m}$	(22)	$C_{eq} = \sum_m^M \sum_n^{N_m} C_{n,m}$	(23)

The equivalent impedance of the feeders is common in the voltage drop and the power loss #1 technique, as they consider the equivalent impedance being the impedance in parallel considered from general electro-technics: $Z_p = \left(\sum_i^m \frac{1}{Z_m} \right)^{-1}$. The power loss #2 method suggests in contrast that the impedance of each string should be weighted with the number of WTs in the string and then normalized with the total number of WTs of strings aggregated (20).

The equivalent capacitance of the cables are common for all the mentioned methods and considered to be parallel and thus summed up.

4.2. Developing a π-Equivalent from the Modal Aggregation Technique

For benchmarking purposes of the impedance accuracy of the aggregation techniques mentioned in Section 4.1, the equivalent grid impedance is considered as the receiving port of the AS impedance by the modal aggregation technique:

$$Z_{eq} = \mathbf{Z}_{AS}[1,1] = \mathbf{Z}_{OSS} \tag{24}$$

The admittance matrix is the inverse of $\mathbf{Z}_{AS}$:

$$\mathbf{Y}_{AS} = \mathbf{Z}_{AS}{}^{-1} \tag{25}$$

Because of the asymmetric properties of $\mathbf{Z}_{AS}$, it is proposed to develop a π-equivalent by averaging the respective reciprocal element of $\mathbf{Z}_{AS}$:

$$\mathbf{Z}_\Pi = \begin{bmatrix} \mathbf{Y}_{AS}[0,0] & \frac{\mathbf{Y}_{AS}[1,0]+\mathbf{Y}_{AS}[0,1]}{2} \\ \frac{\mathbf{Y}_{AS}[1,0]+\mathbf{Y}_{AS}[0,1]}{2} & \mathbf{Y}_{AS}[1,1] \end{bmatrix}^{-1} \tag{26}$$

By disregarding the asymmetric properties of the modal aggregated impedance, it is obvious that some information of the internal dynamics of the collector system is disregarded as well. It, however, allows benchmarking the modal aggregation technique against the other aggregation techniques by time-domain simulations in an immediate manner.

5. Results

The two-norm of the error matrix of the modal aggregation technique and the associated π-equivalent for each of the aggregation techniques are compared. The results are found in Table 4 and scaled in milliSiemens:

Table 4. Comparison of the two-norm error matrices, $||Y_{Aggr.} - Y_{modal}||_2$, in milisiemens.

Case	Voltage Drop	Power Loss #1	Power Loss #2
1	408.29	0.80	0.80
2	1170.77	1.90	2.08
3	227.79	1.19	1.19
4	3238.18	24.37	1.51
2*	510.52	1816.51	2.41
4*	1258.84	2041.78	1.22
Average	1135.73	647.76	1.53

It is observed that the PL2 aggregation technique is by far the most precise aggregation technique with respect to the two-norm, deviating in average by 1.53 mS.

The equivalent impedances are calculated with respect to (26) and (15)–(23) for each case study presented in Section 3. A comparison of the impedances is given in Figure 7 where the modal impedance is given by (24).
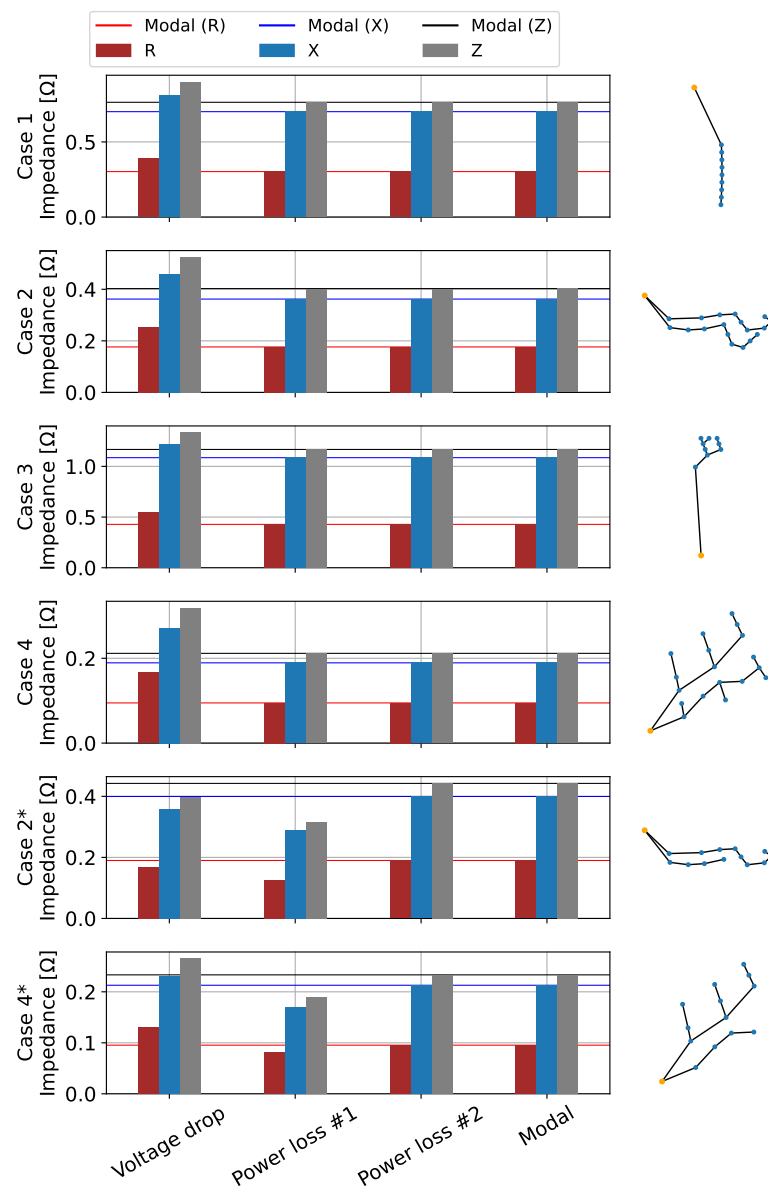
Figure 7. Equivalent impedance calculation and comparison of the investigated aggregation techniques to the modal equivalent of Z_{OSS}.

The voltage drop technique differs from the modal aggregation technique in all cases. The power loss techniques match the modal aggregation technique in all cases except for power loss #1 in case 2* and 4*. The discrepancy is due to the asymmetric number of wind turbines in the individual aggregated string. It is thus clear that the power loss #2 technique is the only technique that matches with the modal aggregation technique in all test systems regardless of branches, multi-string aggregation, or asymmetric string properties.

The equivalent impedance of the respective collector systems and aggregation technique allows a study of the accuracy of time-domain simulations against the detailed model. Figure 8 shows two selected cases (the rest can be found in Appendix A). For test systems, where the number of strings is greater than one, i.e., $M > 1$, results from an aggregated model with individual string aggregation (ISA) are plotted additionally.

All aggregation techniques match the active power response quite well in general. Only during the power reversal post-fault in the beginning of the recovery period, a difference is noted. Except for the VD, there is in general a reasonable match in reactive power. However, the asymmetric case test 4* shows some noticeable deviation. In general, the currents show a larger discrepancy. Case 1 (single string with radial configuration) shows a relatively

large post fault deviation where all the other tests show a fair match. In most cases, the transients when recovering from the fault show deviations in peak values. During the fault, only a remarkable mismatch in asymmetric string configurations (test 2* and 4*) has been identified. Voltage similarity is satisfying.
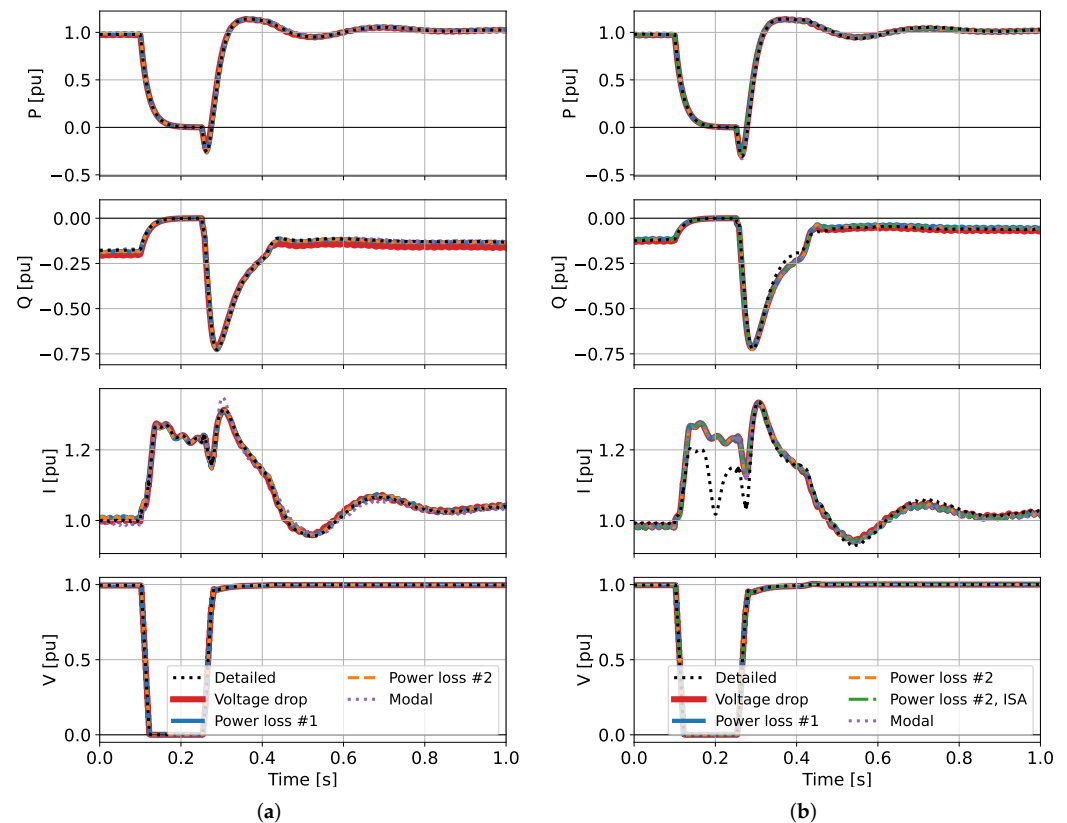

Figure 8. Selected time-domain simulations of case studies. All case studies are contained in the Appendix A. (**a**) Time-domain simulation results for case 3. (**b**) Time-domain simulation results for case 4*.

The error, $\varepsilon = |x_{technique} - x_{detailed}|$, of the aggregation techniques are plotted and can be found in the Appendix B. To investigate the performance of the aggregation techniques further, the error is quantified by an RMS of the error:

$$RMS = \sqrt{\frac{1}{T} \sum_{t}^{T} \varepsilon^2(t)} \tag{27}$$

The RMS errors are found in the Table 5, where the best performing aggregation technique for active power, reactive power, current, and voltage for the respective tests is noted.

The power loss aggregation technique is best in general. It is also seen that there is no effective difference in PL1 and PL2, except for cases of asymmetric strings. In such cases, PL2 matches the best. In cases of more strings than 1, $M > 1$, it is generally seen that it is best to aggregate each string individually. However, ISA does not have any major effect in test 2 (two symmetric strings, no branches). In contrast, ISA has a remarkable effect in test 4 (two symmetric strings, branches). ISA has mixed results when it comes to asymmetric strings; PL2^{ISA} is best in test 2* but underperforms a bit in test 4*.

The π-equivalent model by the modal aggregation technique is in general performing well in comparison as it reaches an average matching ISA and beats VD and PL1, even

though the ISA neglects some dynamic behavior stored in the eigenvalues by averaging the transfer admittance.

Table 5. RMS errors of measurements [%].

Case	Measure	VD	PL1	PL2	PL2^{ISA}	Modal	Best
1	**P**	2.35	2.91	2.91	2.91	2.86	VD
	Q	4.80	2.92	2.92	2.92	2.90	Modal
	I	2.06	1.30	1.30	1.30	1.30	PL1, PL2, PL2^{ISA}, Modal
	V+	0.25	0.15	0.15	0.15	0.15	PL1, PL2, PL2^{ISA}, Modal
2	**P**	4.22	4.56	4.56	4.56	4.62	VD
	Q	3.35	2.69	2.69	2.69	2.73	PL1, PL2, PL2^{ISA}
	I	1.13	1.11	1.11	1.10	1.12	PL2^{ISA}
	V+	0.38	0.32	0.32	0.32	0.33	PL1, PL2, PL2^{ISA}
3	**P**	0.88	0.47	0.47	0.47	1.22	PL1, PL2, PL2^{ISA}
	Q	2.22	0.43	0.43	0.43	0.65	PL1, PL2, PL2^{ISA}
	I	0.43	0.52	0.52	0.52	0.87	VD
	V+	0.12	0.03	0.03	0.03	0.04	PL1, PL2, PL2^{ISA}
4	**P**	4.05	4.83	4.88	2.89	4.88	PL2^{ISA}
	Q	3.18	2.68	2.70	1.81	2.70	PL2^{ISA}
	I	1.00	0.90	0.90	0.68	0.90	PL2^{ISA}
	V+	0.36	0.31	0.31	0.22	0.31	PL2^{ISA}
2*	**P**	2.84	4.51	2.90	2.18	2.83	PL2^{ISA}
	Q	1.54	2.66	1.59	1.18	1.56	PL2^{ISA}
	I	1.56	1.92	1.57	1.25	1.55	PL2^{ISA}
	V+	0.13	0.19	0.13	0.10	0.13	PL2^{ISA}
4*	**P**	1.37	1.57	0.76	1.84	0.76	PL2, Modal
	Q	1.53	1.75	1.56	1.70	1.56	VD
	I	4.04	4.06	4.01	4.06	4.01	PL2, Modal
	V+	0.14	0.15	0.14	0.15	0.14	PL2, Modal
Average		**1.83**	**1.79**	**1.62**	**1.48**	**1.67**	**PL2**

6. Discussion

The power loss aggregation technique is proven to be the best aggregation technique, and ISA is the optimal approach in most cases. The basis of the assumptions for the modal aggregation technique are discussed in this section. In Section 6.1, the assumption of equal current injection is discussed and how non-equal current injections impact the DCFR. In Section 6.2, the DCFR is investigated with respect to higher frequencies to demarcate the validity of the aggregation. In Section 6.3, the sensitivity of DCFR is elaborated with respect to the impedance magnitude.

6.1. Equal Current Injection–Monte Carlo Simulation

The assumptions of the equal current distribution from (11) can be argued to be naive. Monte Carlo simulation (MCS) can be a numerical support and justification of the assumptions of equally distributed currents.

In the MCS presented, the dominant contribution factor ratio (DCFR) is considered from 100,000 samples, while randomizing the current magnitude uniformly distributed in [0.1, 1.0] and phase angle uniformly distributed in [$-60°$, $60°$]. The dominant contribution factor ratio is defined as:

$$DCFR = \frac{m_0}{m_1} \tag{28}$$

The DCFR is shown in Figure 9. It is seen that the case studies have a great impact on the distribution of DCFR, but the DCFR is in either case very large and the impact of non-equal current injections are thus negligible. The lowest DCFR observed is 2665.5 for case 2*. It is noticed that asymmetric variants of the corresponding case study has a negative

impact on the DCFR distribution, meaning that the aggregation would be more challenging.
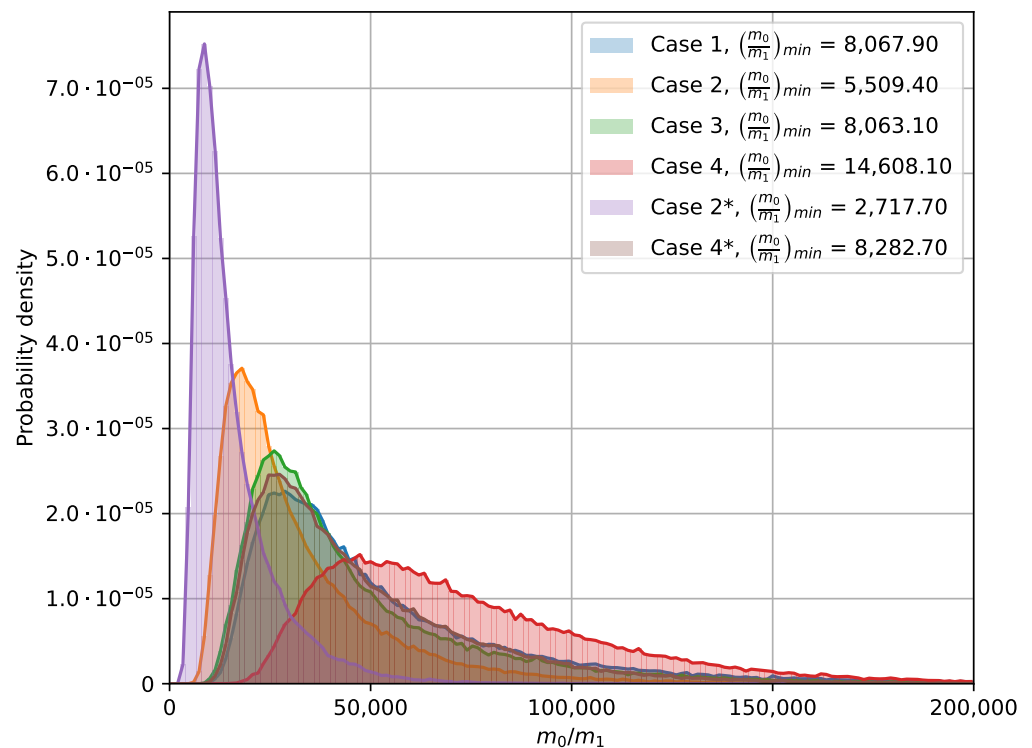

Figure 9. Dominant contribution factor ratio comparison.

The impact on the modal turn ratio p of non-equal current injections is considered by MCS. In Figure 10a,b, the magnitude and phase angle of the modal turn ratio is considered, respectively. The magnitude of the modal turn ratio follows by high accuracy the rule, $p = \sqrt{N}$, and seems to equal the mean of the distribution (except for case 3, which is slightly right-skewed). The phase angles do not differ much in most cases and are considered negligible. There is no clear pattern of impact of asymmetric strings, nor aggregating more strings than 1.

Non-equal current injections are thus considered not to have a devastating impact on the DCFR, and the modal aggregation technique thus holds as a verification model, as the contribution factors of the passive collector system do not depend on load flow conditions.
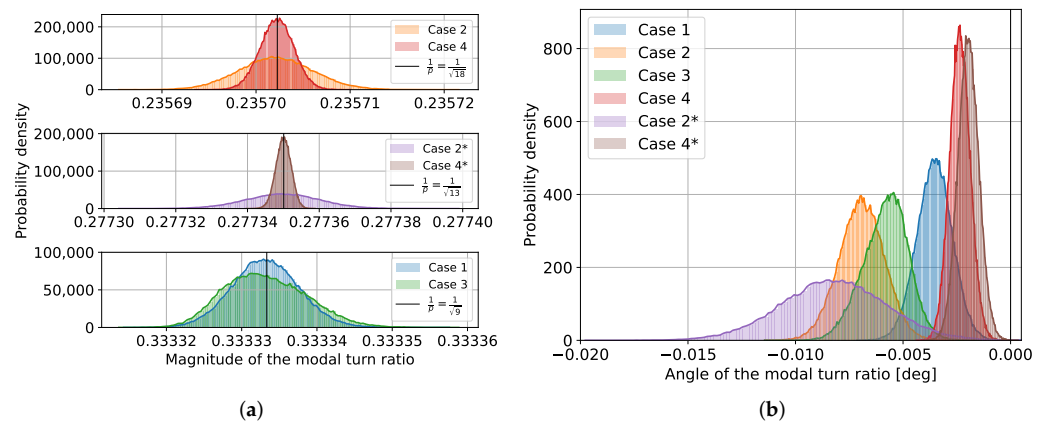

Figure 10. Magnitude and angle distributions of the modal turn ratio p from Monte Carlo simulations. (**a**) Magnitude distributions. (**b**) Angle distributions.

6.2. DCFR and Higher Frequencies

The harmonic impedance is of great importance when performing detailed studies. The DCFR is studied with respect to higher frequencies and plotted in Figure 11. Figure 11a, ranging 50–400 Hz, is a zoomed version of Figure 11b, ranging 50–2500 Hz. In Figure 11a, it is observed that the intersection of the DCFR and the tentative DCFR limit varies with respect to the case study. It is in general observed that the case studies with multiple strings are more impacted by higher frequencies. This fact supports the ISA approach.

It was investigated whether another DCFR would show itself for higher frequencies. This is, however, rejected by the plot in Figure 11b as no other DCFR reaches over the tentative DCFR limit.
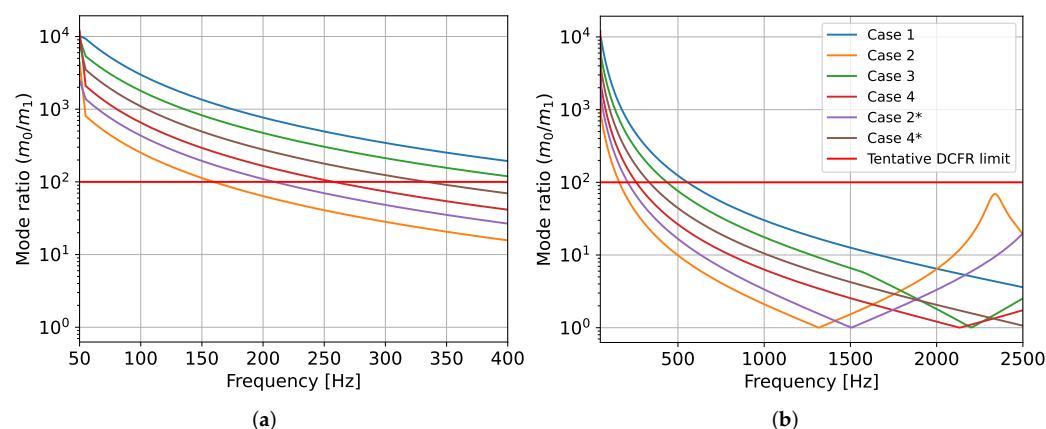

Figure 11. Dominant contribution factor ratio comparison sensitive to distance factor. (**a**) Frequencies $\in [50; 400]$ Hz. (**b**) Frequencies $\in [50; 2500]$ Hz.

It is thus clear that studies of harmonic emissions from converter switching frequencies of around 1500 Hz or fast transients like switching impulses with a front time of 20 kHz [43] are incompatible with an aggregated model. Using detailed models should thus be used for studies for high frequencies.

In an aggregation perspective, modelling higher frequencies would require a higher order of the RLC equivalent component to be realized.

6.3. Impedance Magnitude Distance (Mode Ratio)

Anholt Wind Farm was commissioned in 2013 and WTs have grown in size and capacity since then. This development increases the distance between the individual turbines for a better energy yield. As 66 kV is currently a new standard voltage for collector systems, new cable data will dictate the impedance characteristics of the collector system. However, the DCFR is studied by multiplying the length of all cable sections with a distance factor. The results are shown in Figure 12.

The DCFR decreases as the network impedance increases by the distance factor. Case studies with multiple strings tend to decrease more rapidly in DCFR in contrast to the single string systems. For instance, Figure 12 shows that Case 2 is not accurate when the distance factor is bigger than 8 (based on a tentative threshold for DCFR = 100). It is also noticed that the situation is even worse for asymmetrical cases, i.e., cases 2* and 4*.

In Figure 13, the time-domain simulation of case 2 with a distance factor of 15 is plotted to emphasize the validity of aggregation fails, as the DCFR is very low ($\frac{m_0}{m_1} \approx 27.5$) and the second-largest mode is no more negligible.

The detailed model has a little oscillation in active power post fault as it recovers. The modal and the power loss techniques are plotted on top of each other and fail to replicate this behavior. The voltage drop technique fails to stabilize before the detailed model.
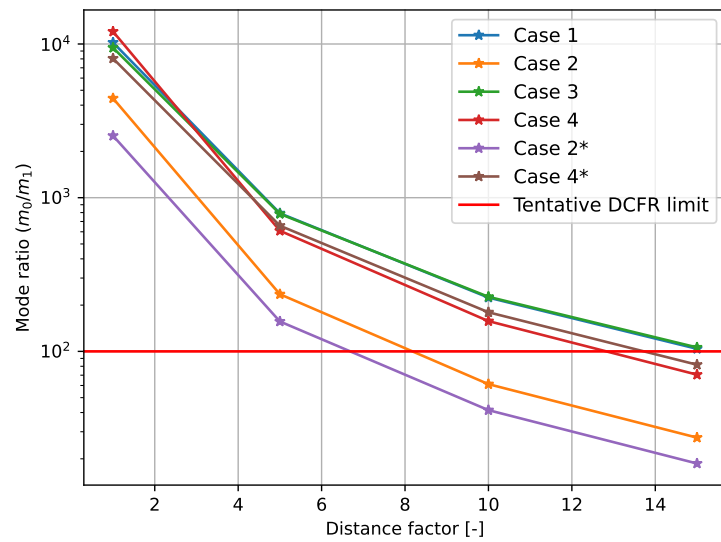
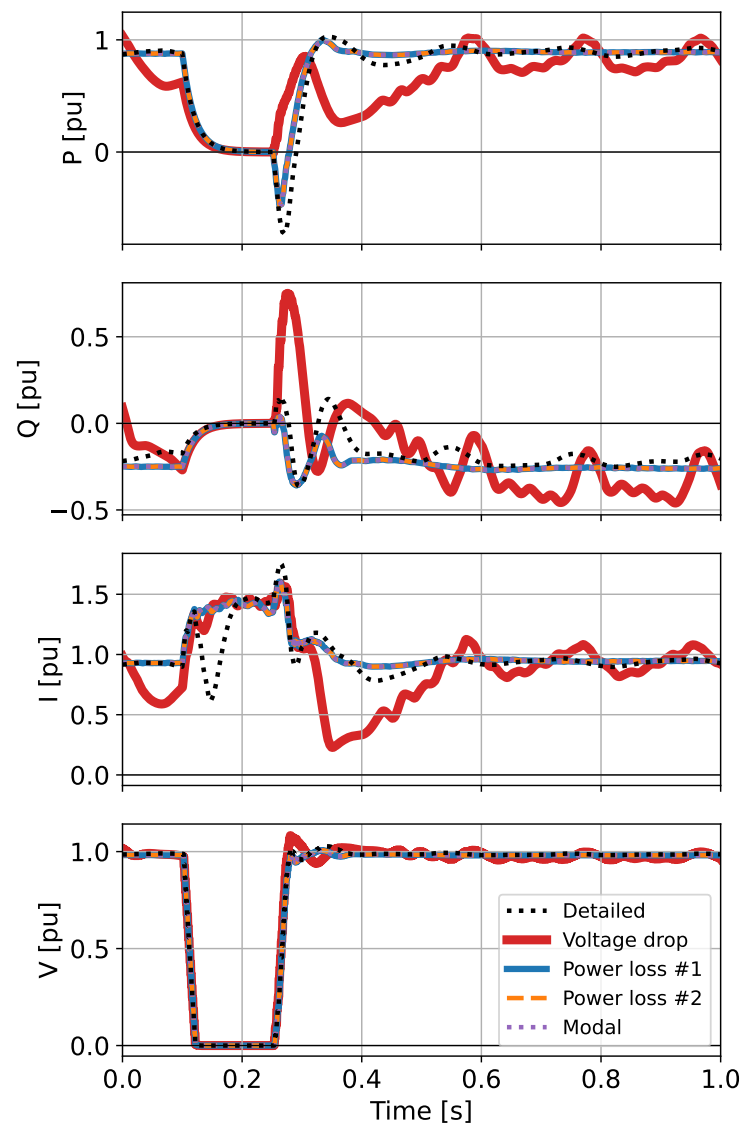**Figure 12.** Mode ratio with respect to distance factor.

Figure 13. Time-domain simulation of case 2 with distance factor = 15.

7. Conclusions and Future Works

Aggregation of the collector system of an OWF is beneficial as it is not dependent on the type of the wind turbine. It is not dependent on the detailed model of the wind turbine either, i.e., the aggregation does not change whether it is a black-box, white-box, or a grey-box model.

Case studies of different collector system layouts were derived from the Anholt Wind Farm and aggregated with the voltage drop, power loss, and modal aggregation techniques. The results from a dynamic simulation of a 3-phase to ground fault showed that the power loss technique is the most accurate aggregation technique for collector systems.

The impact of unequal currents from the wind turbines is shown to be negligible and, therefore, the same aggregation can be used for different operating conditions (e.g., different wind speeds).

Aggregation is a model order reduction as the entire array cable system is simplified into one cable section. Therefore, the aggregated model is expected not to be able to represent certain dynamics. It is shown that the frequency and length of array cables have a big impact on the validity of the aggregation in contrast.

Future work will thus look into: (1) impact of the aggregation on the stability and reliability of power systems, (2) defining a DCFR-based validity threshold, (3) developing an aggregation model based on the exact modal aggregation technique (e.g., a higher order RLC component model or an active impedance equivalent), (4) developing multi-port aggregated models based on the dominant contribution factors or nodes of interest, (5) the impact on the mix of cable types in the aggregated string and impact of the string layout, i.e., branching; (6) quantifying the impact on the grid voltage from, (7) benchmark performance of aggregation techniques for meshed networks or wind farms with loops against a modal aggregation technique-derived model.

Author Contributions: Conceptualization, M.K.B.; methodology, M.K.B. and B.V.; formal analysis, all; investigation, M.K.B. and B.V.; writing—original draft, B.V.; writing—review and editing, all; supervision, M.K.B. and Ł.K. All authors have read and agreed to the published version of the manuscript.

Data Availability Statement: Not applicable.

Conflicts of Interest: The authors declare no conflict of interest.

Abbreviations and Subscripts

The following abbreviations are used in this manuscript:

ADN	Active Distribution Network
agg	Aggregated
AS	Aggregated System
CF	Contribution Factor
CS	Collector System
DCFR	Dominant Contribution Factor Ratio
ISA	Individual String Aggregation
MCS	Monte Carlo Simulation
OSS	Offshore Substation
OWF	Offshore Wind Farm
PL	Power Loss
VD	Voltage Drop
WT	Wind Turbine

Symbols

The following symbols are used in this manuscript:

V'	Representation of V in the modal domain
X	Matrix or vector formed of elements x_i
ε	Approximation error
Λ	Eigenvalues in matrix form (diagonally placed)
r	Right eigenvector
R	Right eigenvectors in matrix form
V	Voltage
I	Current
Z	Impedance
C	Capacitance
M	Number of feeders connected to the offshore substation
p	Modal turn ratio
m	Contribution factor or m'th feeder
$DCFR$	Dominant Capacity Factor Ratio

Appendix A. Time-Domain Simulation Results for All Case Studies

The active power, reactive power, current, and voltage is plotted in each row respectively for each test in the respective column.
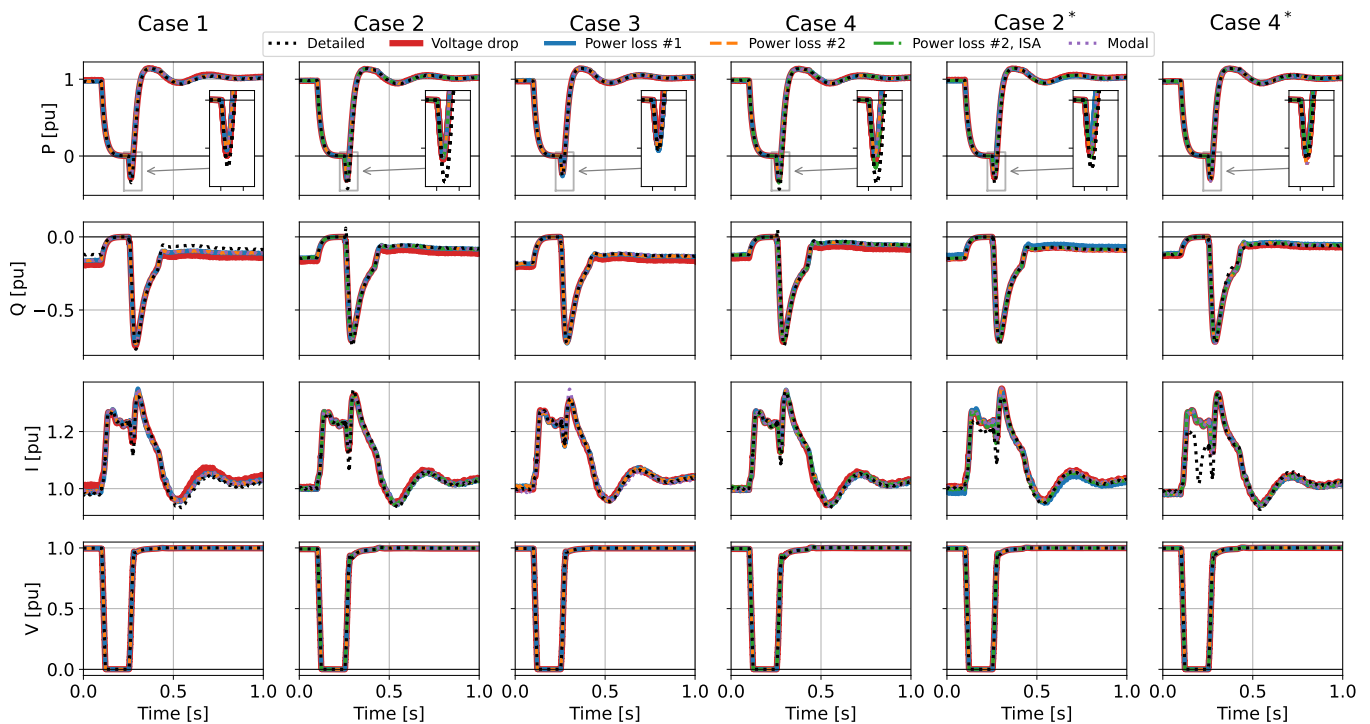

Figure A1. Time-domain simulation results from PSCAD for all case studies.

Appendix B. Errors of Time-Domain Simulation Results for All Case Studies
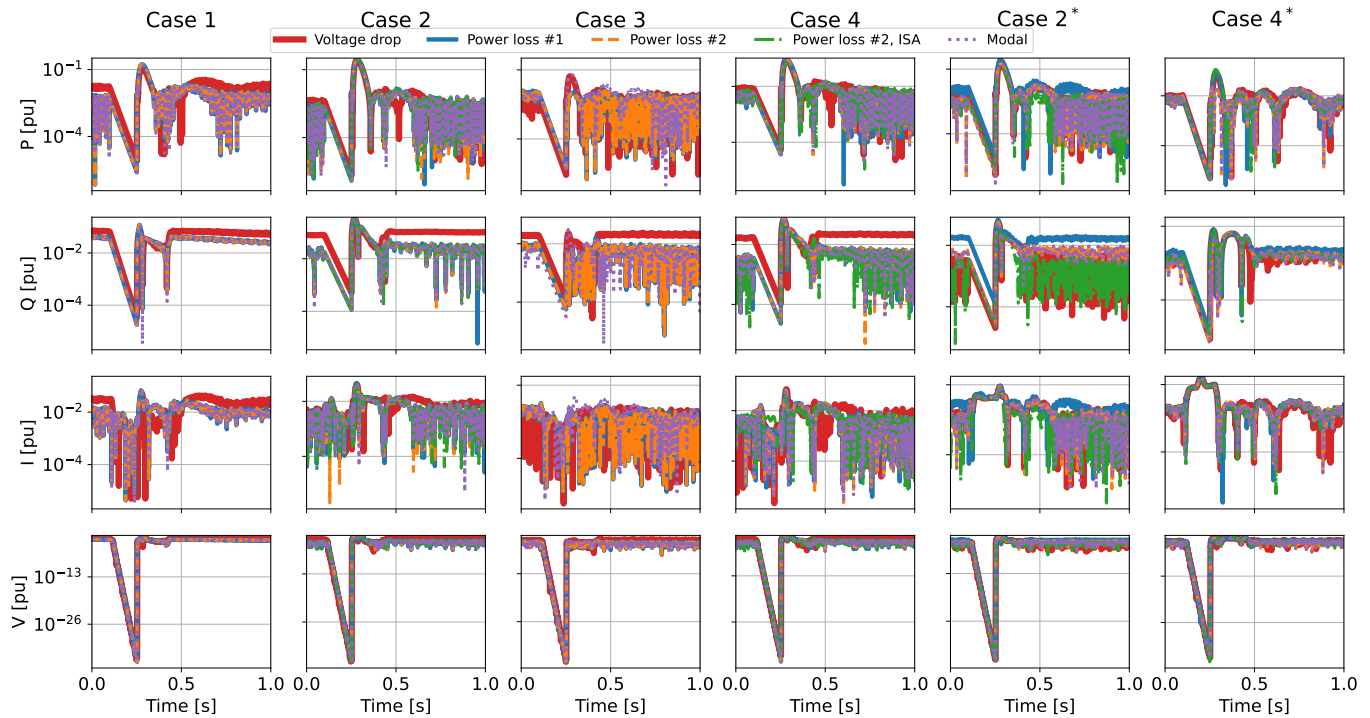

Figure A2. Errors plotted in log-scale from time-domain simulation results for all case studies with respect to the detailed equivalent of the case study.

References

1. Chedid, R.; LaWhite, N.; Ilic, M. A Comparative Analysis of Dynamic Models for Performance Calculation of Grid-Connected Wind Turbine Generators. *Wind Eng.* **1993**, *17*, 168–182.
2. Rahman, M.T.; Hasan, K.N.; Sokolowski, P. Evaluation of wind farm aggregation using probabilistic clustering algorithms for power system stability assessment. *Sustain. Energy Grids Netw.* **2022**, *30*, 100678. [CrossRef]
3. Milanovic, J.V.; Mat Zali, S. Validation of equivalent dynamic model of active distribution network cell. *IEEE Trans. Power Syst.* **2013**, *28*, 2101–2110. [CrossRef]
4. Li, H.; Chen, Z. Overview of different wind generator systems and their comparisons. *IET Renew. Power Gener.* **2008**, *2*, 123–138. [CrossRef]
5. Fernández, L.M.; García, C.A.; Saenz, J.R.; Jurado, F. Equivalent models of wind farms by using aggregated wind turbines and equivalent winds. *Energy Convers. Manag.* **2009**, *50*, 691–704. [CrossRef]
6. Shafiu, A.; Anaya-Lara, O.; Bathurst, G.; Jenkins, N. Aggregated wind turbine models for power system dynamic studies. *Wind Eng.* **2006**, *30*, 171–186. [CrossRef]
7. Akhmatov, V.; Knudsen, H. An aggregate model of a grid-connected, large-scale, offshore wind farm for power stability investigations-importance of windmill mechanical system. *Fuel Energy Abstr.* **2003**, *44*, 161. [CrossRef]
8. Tapia, G.; Tapia, A.; Ostolaza, J.X. Two alternative modeling approaches for the evaluation of wind farm active and reactive power performances. *IEEE Trans. Energy Convers.* **2006**, *21*, 909–920. [CrossRef]
9. Windenergie Report Deutschland 2018. Available online: https://publica.fraunhofer.de/entities/publication/c3cff226-62e8-4fa2 -b9c2-c2e18fa9328a/details (accessed on 17 October 2022).
10. Conroy, J.; Watson, R. Aggregate modelling of wind farms containing full-converter wind turbine generators with permanent magnet synchronous machines: Transient stability studies. *IET Renew. Power Gener.* **2009**, *3*, 39–52. [CrossRef]
11. Kunjumuhammed, L.P.; Pal, B.C.; Oates, C.; Dyke, K.J. The Adequacy of the Present Practice in Dynamic Aggregated Modeling of Wind Farm Systems. *IEEE Trans. Sustain. Energy* **2017**, *8*, 23–32. [CrossRef]
12. Marinopoulos, A.; Pan, J.; Zarghami, M.; Reza, M.; Yunus, K.; Yue, C.; Srivastava, K. Investigating the impact of wake effect on wind farm aggregation. In Proceedings of the 2011 IEEE Pes Trondheim Powertech: The Power of Technology for a Sustainable Society, Powertech, Trondheim, Norway, 19–23 June 2011; p. 6019323. [CrossRef]
13. Ruan, J.Y.; Lu, Z.X.; Qiao, Y.; Min, Y. Analysis on Applicability Problems of the Aggregation-Based Representation of Wind Farms Considering DFIGs' LVRT Behaviors. *IEEE Trans. Power Syst.* **2016**, *31*, 4953–4965. [CrossRef]

14. Fernandez, L.M.; Garcia, C.A.; Jurado, F.; Saenz, J.R. Aggregation of doubly fed induction generators wind turbines under different incoming wind speeds. In Proceedings of the 2005 IEEE Russia Power Tech, Powertech, St. Petersburg, Russia, 27–30 June 2005; p. 4524685. [CrossRef]

15. Liu, H.; Chen, Z. Aggregated modelling for wind farms for power system transient stability studies. In Proceedings of the 2012 Asia-pacific Power and Energy Engineering Conference, Shanghai, China, 27–29 March 2012; p. 6307118. [CrossRef]

16. Fernández, L.M.; Jurado, F.; Saenz, J.R. Aggregated dynamic model for wind farms with doubly fed induction generator wind turbines. *Renew. Energy* **2008**, *33*, 129–140. [CrossRef]

17. Mercado-Vargas, M.J.; Gómez-Lorente, D.; Rabaza, O.; Alameda-Hernandez, E. Aggregated models of permanent magnet synchronous generators wind farms. *Renew. Energy* **2015**, *83*, 1287–1298. [CrossRef]

18. Wang, H.; Buchhagen, C.; Sun, J. Methods to aggregate turbine and network impedance for wind farm resonance analysis. *IET Renew. Power Gener.* **2020**, *14*, 1304–1311. [CrossRef]

19. Cheng, X.; Lee, W.J.; Sahni, M.; Cheng, Y.; Lee, L.K. Dynamic equivalent model development to improve the operation efficiency of wind farm. In Proceedings of the 2015 IEEE/IAS 51st Industrial and Commercial Power Systems Technical Conference, I and Cps, Calgary, AB, Canada, 5–8 May 2015; p. 7266410. [CrossRef]

20. Mat Zali, S.; Milanovic, J.V. Generic model of active distribution network for large power system stability studies. *IEEE Trans. Power Syst.* **2013**, *28*, 3126–3133. [CrossRef]

21. Brogan, P. The stability of multiple, high power, active front end voltage sourced converters when connected to wind farm collector systems. *EPE Wind Energy Chapter Semin.* **2010**, 1–6. [CrossRef]

22. Martínez-Turégano, J.; Añó-Villalba, S.; Bernal-Perez, S.; Blasco-Gimenez, R. Aggregation of type-4 large wind farms based on admittance model order reduction. *Energies* **2019**, *12*, 1730. [CrossRef]

23. Zou, J.; Peng, C.; Xu, H.; Yan, Y. A Fuzzy Clustering Algorithm-Based Dynamic Equivalent Modeling Method for Wind Farm with DFIG. *IEEE Trans. Energy Convers.* **2015**, *30*, 1329–1337. [CrossRef]

24. Muljadi, E.; Butterfield, C.P.; Ellis, A.; Mechenbier, J.; Hochheimer, J.; Young, R.; Miller, N.; Delmerico, R.; Zavadil, R.; Smith, J.C. Equivalencing the collector system of a large wind power plant. In Proceedings of the 2006 IEEE Power Engineering Society General Meeting, Montreal, QC, Canada, 18–22 June 2006; p. 1708945. [CrossRef]

25. Muljadi, E.; Pasupulati, S.; Ellis, A.; Kosterov, D. Method of equivalencing for a large wind power plant with multiple turbine representation. In Proceedings of the IEEE Power and Energy Society 2008 General Meeting: Conversion and Delivery of Electrical Energy in the 21st Century, Pittsburgh, PA, USA, 20–24 July 2008; p. 4596055. [CrossRef]

26. Abbes, M.; Allagui, M.; Hasnaoui, O.B. An aggregate model of PMSG-based, grid connected wind farm: Investigation of LVRT capabilities. In Proceedings of the 2015 6th International Renewable Energy Congress, Irec 2015, Sousse, Tunisia, 24–26 March 2015; p. 7110976. [CrossRef]

27. Ali, M.; Ilie, I.S.; Milanovic, J.V.; Chicco, G. Wind farm model aggregation using probabilistic clustering. *IEEE Trans. Power Syst.* **2013**, *28*, 309–316. [CrossRef]

28. Kocewiak, L.H.; Hjerrild, J.; Bak, C.L. Wind farm structures' impact on harmonic emission and grid interaction. In Proceedings of the European Wind Energy Conference and Exhibition 2010, Ewec 2010, Warszawa, Poland, 20–23 April 2010; Volume 4, pp. 2829–2836.

29. Pöller, M.; Achilles, S. Aggregated Wind Park Models for Analyzing Power System Dynamics. In Proceedings of the 4th International Workshop on Large-Scale Integration of Wind Power and Transmission Networks for Offshore Wind Farms, Billund, Denmark, 2014.

30. Quinonez-Varela, G.; Ault, G.W.; Anaya-Lara, O.; McDonald, J.R. Electrical collector system options for large offshore wind farms. *IET Renew. Power Gener.* **2007**, *1*, 107–114. [CrossRef]

31. Lin, W.; Wen, J.; Liang, J.; Cheng, S.; Yao, M.; Li, N. A Three-Terminal HVDC System to Bundle Wind Farms with Conventional Power Plants. *IEEE Trans. Power Syst.* **2013**, *28*, 2292–2300. [CrossRef]

32. Dutta, S.; Overbye, T.J. A clustering based wind farm collector system cable layout design. In Proceedings of the 2011 IEEE Power and Energy Conference at Illinois, Peci 2011, Urbana, IL, USA, 25–26 February 2011; p. 5740480. [CrossRef]

33. Kocewiak, Ł.H.; Kramer, B.L.Ø.; Holmstrøm, O.; Jensen, K.H.; Shuai, L. Resonance damping in array cable systems by wind turbine active filtering in large offshore wind power plants. *IET Renew. Power Gener.* **2017**, *11*, 1069–1077. [CrossRef]

34. Chow, J.H. *Power System Coherency and Model Reduction*; Springer: New York, NY, USA, 2013.

35. Sundararajan, D. *Introductory Circuit Theory*; Springer: Cham, Switzerland, 2020.

36. Chechurin, V.L.; Korovkin, N.V.; Hayakawa, M.; Hayakawa, M. *Inverse Problems in Electric Circuits and Electromagnetics*; Springer: New York, NY, USA, 2007.

37. Kundur, P.S. *Power System Stability and Control*; McGraw-Hill: New York, NY, USA, 1994.

38. Ørsted: Anholt Offshore Wind Farm. Available online: https://orstedcdn.azureedge.net/-/media/www/docs/corp/com/our-business/wind-power/wind-farm-project-summary/anholt_uk_2018.ashx?la=en&rev=3b2f175b341e4ca2b906bf2a2ff68c8f&hash=51B4609E53A631D29E0EF49936C33A84 (accessed on 26 September 2022).

39. 6–36 kV Medium Voltage Underground Power Cables. Available online: https://www.powerandcables.com/wp-content/uploads/2016/12/Nexans-6-33kV-Medium-High-Voltage-Underground-Power-Cables.pdf (accessed on 18 October 2022).

40. *IEC 61400-27-1 Ed. 2*; Wind Turbines-Part 27-1: Electrical Simulation Models for Wind Power Generation—Wind Turbines. International Electrotechnical Commission: Geneva, Switzerland, 2020.

41. PSCAD Type 4 Wind Turbine Generators. Available online: https://www.pscad.com/knowledge-base/article/227 (accessed on 25 August 2022).
42. Kocewiak, L. Harmonics in Large Offshore Wind Farms. Ph.D. Dissertation, Department of Energy Technology at Aalborg University, Aalborg, Denmark, 2012.
43. *60060-1:2011*; High-Voltage Test Requirements, Part 1: General Definitions and Test Requirements. International Electrotechnical Commission (IEC): Geneva, Switzerland, 2011.